CHAPTER 7: THE CRYSTALLINE SOLID STATE

7.1   **a.** O_h **b.** D_{4h} **c.** O_h **d.** T_d

    e.   The image in Figure 7.10, which has D_{3d} symmetry, actually consists of three unit cells. For an image of a single unit cell, which has point group C_{2h}, see page 556 in the Greenwood and Earnshaw reference in the "General References" section.

7.2   The unit-cell dimension is $2r$, the volume is $8r^3$. Since this cell contains one molecule whose volume is $4/3 \pi r^3$, the fraction occupied is $\dfrac{4/3\pi r^3}{8r^3} = 0.524 = 52.4\%$.

7.3   The unit-cell length for a primitive cubic cell is $2r$. Using the Pythagorean theorem, we can calculate the face diagonal as $\sqrt{(2r)^2 + (2r)^2} = 2.828r$ and the body diagonal as $\sqrt{(2.828r)^2 + (2r)^2} = 3.464r$. Each corner atom contributes r to this distance, so the diameter of the body center is $1.464\ r$ and the radius is $0.732\ r$, 73.2% of the corner atom size.

7.4   **a.**   A face-centered cubic cell is shown preceding Exercise 7.1 in Section 7.1.1. The cell contains $6 \times \frac{1}{2} = 3$ atoms at the centers of the faces and $8 \times \frac{1}{8} = 1$ atom at the corners, a total of 4 atoms. The total volume of these 4 atoms $= 4 \times \dfrac{4}{3}\pi r^3 = \dfrac{16}{3}\pi r^3$, where r is the radius of each atom (treated as a sphere).

As can be seen in the diagram, the diagonal of a face of the cube $= 4r$. By the Pythagorean theorem, the dimension (length of a side) of the cube $= \dfrac{\text{diagonal}}{\sqrt{2}} = \dfrac{4r}{\sqrt{2}}$.

The volume of the cube, therefore, $= \left(\dfrac{4r}{\sqrt{2}}\right)^3 = \dfrac{32r^3}{\sqrt{2}}$.

The ratio $\dfrac{\text{volume of spheres}}{\text{volume of cube}} = \dfrac{\left(\dfrac{16}{3}\pi r^3\right)}{\left(\dfrac{32r^3}{\sqrt{2}}\right)} = 0.740$.
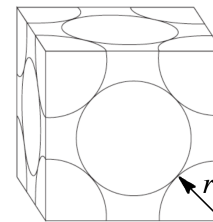
Therefore, 74.0% of the volume of the cube is occupied by the spheres.

b.   In a body-centered cube, the unit cell contains 1 atom in the center of the cube and $8 \times \frac{1}{8} = 1$ atom at the corners, a total of 2 atoms. The total volume of these 2 atoms $= 2 \times \dfrac{4}{3}\pi r^3 = \dfrac{8}{3}\pi r^3$, where r is the radius of each atom.

Because atoms touch along the diagonal, the diagonal of the cube $= 4r$. Using the Pythagorean theorem, it can be shown that the dimension of the cube $= \dfrac{\text{diagonal}}{\sqrt{3}} = \dfrac{4r}{\sqrt{3}}$.

$$\text{Therefore, the volume of the cube} = \left(\frac{4r}{\sqrt{3}}\right)^3 = \frac{64r^3}{3\sqrt{3}}$$

$$\text{The ratio} \ \frac{\text{volume of spheres}}{\text{volume of cube}} = \frac{\left(\frac{8}{3}\pi r^3\right)}{\left(\frac{64r^3}{3\sqrt{3}}\right)} = 0.680 \text{ or } 68.0\%$$

7.5 In the table below, CaF_2 is considered to have a fluoride ion in the body center of the overall unit cell and calcium ions in the body centers of the subunits (labeled "Internal").

Compound	Corners	Edges	Face Centers	Body Centers	Internal	Total	Type
NaCl cations	8 × 1/8		6 × 1/2			4	MX
NaCl anions		12 × 1/4		1 × 1		4	MX
CsCl cations	8 × 1/8					1	MX
CsCl anions				1 × 1		1	MX
CaF$_2$ cations					4 × 1	4	MX$_2$
CaF$_2$ anions	8 × 1/8	12 × 1/4	6 × 1/2	1 × 1		8	MX$_2$

7.6 LiBr has a formula weight of 86.845, and the unit cell contains four cations and four anions (or four formula units per molecular unit cell).

$$\frac{86.845 \text{ g mol}^{-1}}{3.464 \text{ g cm}^{-3}} = 25.07 \text{ cm}^3\text{mol}^{-1} \times \frac{10^{-6}\text{m}^3}{\text{cm}^3} = 2.507 \times 10^{-5}\text{m}^3\text{mol}^{-1}$$

$$\frac{2.507 \times 10^{-5}\text{m}^3\text{mol}^{-1}}{6.022 \times 10^{23}\text{units mol}^{-1}} \times \frac{4 \text{ units}}{\text{unit cell}} = \frac{1.665 \times 10^{-28}\text{m}^3}{\text{unit cell}}$$

$$\sqrt[3]{1.665 \times 10^{-28}\text{m}^3} = 5.502 \times 10^{-10}\text{m} = \text{ unit cell length}$$

$$2(r_+ + r_-) = 5.502 \times 10^{-10}\text{m}; \ r_+ + r_- = 2.751 \times 10^{-10}\text{m} = 275.1 \text{ pm}$$

The sum of the ionic radii from Appendix B.1 is 261 pm.

7.7 CsCl has 8 Cl$^-$ at the corners of the unit cell cube, with the Cs$^+$ at the center.
$$r_+/ r_- = 173/167 = 1.04.$$

CaF$_2$ has the same structure in a single cube of F$^-$ ions, but only half the cubes contain Ca^{2+}.
$$r_+/ r_- = 126/119 = 1.06.$$

Both should have coordination number = 12 based on the radius ratios.

7.8   Figure 7.8 shows the zinc blende unit cell, which contains four S atoms (net) in an fcc lattice and four Zn atoms in the body centers of the alternate smaller cubes. The diagrams below are each a view of two layers of such a cell, with • indicating a Zn atom in this layer and a ○ indicating a S atom in the layer below. The next pair of layers either above or below these has the opposite pattern, and the third repeats the original. The fcc lattice pattern can be seen for the Zn atoms (four corners and face center on the top face, four face centers in the middle later, and four corners and face center on the bottom face). Each S atom (and each Zn atom) has two nearest neighbors in the layer above and two in the layer below, in the arrangement for a tetrahedral hole. Extending the patterns below shows the S fcc lattice.
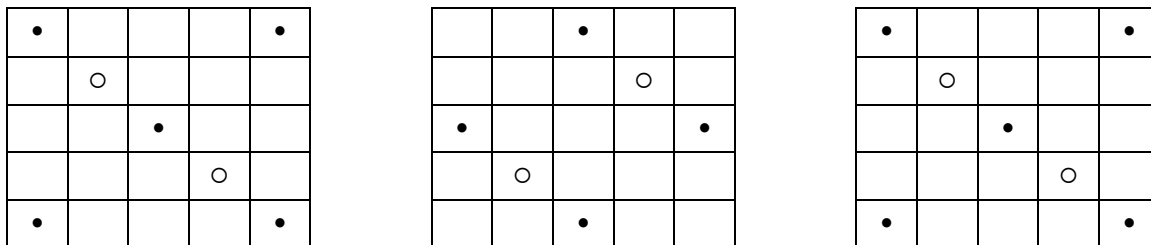
7.9   The graphite layers have essentially the same energy levels as benzene, but each level becomes a wider band because of the large number of atoms. This leads to the energy levels shown at right, with the bands coming from the lowest energy π orbitals filled and those coming from the highest energy π orbitals empty. The difference between the highest occupied and lowest unoccupied bands is small enough to allow conduction electrons to make the jump and the electrons and holes to move within the bands. Conduction perpendicular to the layers is smaller, because there are no direct orbitals connecting them. In polycrystalline graphite, the overall conductance is an average of the two. (The π orbitals of benzene are shown in Figure 13.22.)

π^*

π

C_6H_6 Graphite
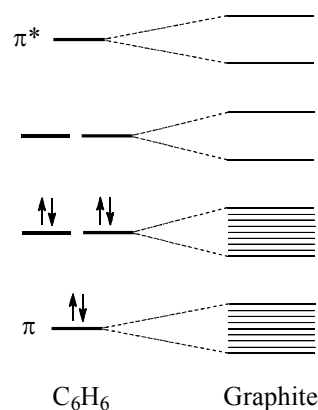
In diamond, each carbon atom has four σ bonds to its nearest neighbors.
The gap between these filled orbitals and the corresponding antibonding orbitals is larger, effectively limiting conductance. The bonding in carbon nanotubes resembles that of graphite, and conductivity is expected. The conductivity of carbon nanotubes is a function of the diameter of the tubes, and spans the range associated with semiconductors to metallic conductors, up to approximately 1000 times the conductivity of copper (Section 8.6.1).

7.10   Solutions of alkali halides in water conduct electricity. This does not prove that they are ionic as solids, but is suggestive of ions in the solid state. Their high melting points are also suggestive of ionic structures, and the molten salts also conduct electricity. Perhaps the most conclusive evidence is from X-ray diffraction studies, in which these compounds show uniform cation—anion distances. If they were molecular species, the interatomic distances within a molecule should be smaller than the interatomic distances between molecules.

7.11   Hg(I) appears in compounds such as Hg_2^{2+} units. The $6s^1\,4f^{14}\,5d^{10}$ structure of Hg^+ forms σ and σ* molecular orbitals from the s atomic orbitals, allowing the two s electrons to pair in the σ orbital for a diamagnetic unit.

7.12 **a.** Forming anions from neutral atoms results in the addition of an electron. More electrons means a larger size, due to increasing electron—electron repulsion. By the same argument,

forming cations from neutral atoms results in removal of an electron and smaller size. The cations have fewer electrons and less electron-electron repulsions.

b. The oxide ion is larger than the fluoride ion because its nuclear charge is smaller; the oxygen nucleus has less attraction for the electrons.

7.13 Radius ratios for the alkali halides, using ionic radii for CN = 6 (Appendix B.1):

Ions	Radii (pm)	Li^+	Na^+	K^+	Rb^+	Cs^+
Radii (pm)		79	107	138	166	181
F^-	119	**0.66**	0.90	1.16	1.39	1.52
Cl^-	167	**0.47**	**0.64**	0.83	0.99	1.08
Br^-	182	**0.43**	**0.59**	0.76	0.91	0.99
I^-	206	0.38	**0.52**	**0.67**	0.81	0.88

These salts all actually exhibit the sodium chloride lattice (CN = 6), and radius ratios between 0.414 and 0.732 are expected (Table 7.1). The seven boldface entries are the only structures correctly predicted on the basis of these data. These data incorrectly predict LiI to have CN = 4, NaF, KCl, KBr, RbCl, RbBr, RbI, CsBr, and CsI to have CN = 8, and KF, RbF, CsF, and CsCl to have CN = 12.

7.14 The interionic distances for salts of the same cation increase as $Br^- > Cl^- > F^-$ as expected on the basis of the increasing sizes of these monoanions with increasing atomic number.
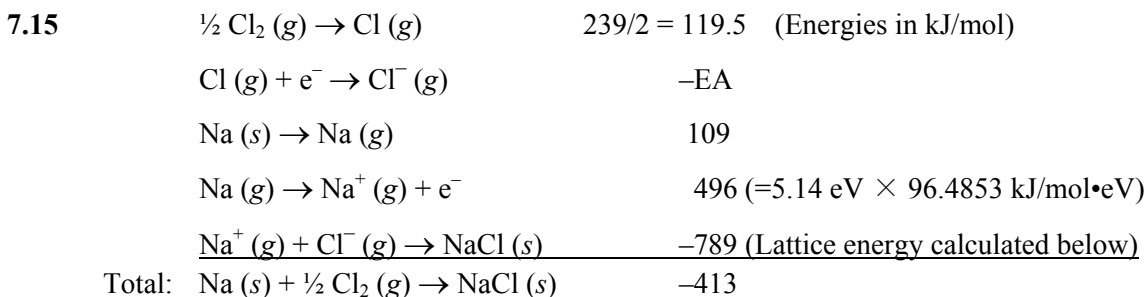
A comparison of these interionic distances with the sum of the corresponding ionic radii is interesting. Ionic radii for CN = 6 are used (Appendix B.1) in determining the sums (pm) below.

Salt	Interionic Distance	Sum of Ionic Radii	Salt	Interionic Distance	Sum of Ionic Radii	Salt	Interionic Distance	Sum of Ionic Radii
LiF	201	198	NaF	231	226	AgF	246	248
LiCl	257	246	NaCl	281	274	AgCl	277	296
LiBr	275	261	NaBr	298	289	AgBr	288	311

It is interesting that only the silver salts exhibit *shorter* interionic distances than predicted by the sum of the ionic radii. As the softness of the anion increases, the absolute contraction of the interionic distance relative to the sum of the ionic radii increases (from only 2 pm (AgF) to 23 pm (AgBr)). This suggests an increasing covalent contribution in the interaction with Ag^+ as the halide softness increases from F^- to Br^-. Estimation of the interionic distance using ionic radii clearly introduces more error as the softness of the interaction towards Ag^+ increases.

For the lithium and sodium salts, the interionic distances are all longer than the sum of the ionic radii. The agreement between the distances on a percentage basis is best for LiF (the interionic distance is 1.5% greater than the sum of the ionic radii) and worst for LiBr (the interionic distance is 5.4% greater than the sum of the ionic radii). The agreement between these values tracks qualitatively with the hard-soft compatibility of these ions. The relative differences in these

distances changes more dramatically with decreasing halide softness for the harder Li^+ (from 1.5% to 5.4%) than with the less hard Na^+ (2.2% to 3.1%).

7.15 $\frac{1}{2}$ Cl_2 $(g) \rightarrow Cl$ (g) 239/2 = 119.5   (Energies in kJ/mol)

Cl $(g) + e^- \rightarrow Cl^-$ (g) $-EA$

Na $(s) \rightarrow Na$ (g) 109

Na $(g) \rightarrow Na^+$ $(g) + e^-$ 496 (=5.14 eV $\times$ 96.4853 kJ/mol•eV)

$\underline{Na^+ (g) + Cl^- (g) \rightarrow NaCl (s) \qquad\qquad -789 \text{ (Lattice energy calculated below)}}$

Total: Na $(s) + \frac{1}{2}$ Cl_2 $(g) \rightarrow NaCl$ (s) -413

EA = 348.5 kJ/mol (The value in Appendix B.3 is 349 kJ/mol.)

$$U = \frac{NMZ_+Z_-}{r_0}\left[\frac{e^2}{4\pi\varepsilon_0}\right]\left(1-\frac{\rho}{r_0}\right) = \frac{6.022\times10^{23}\times1.74756\times1\times(-1)}{274\times10^{-12}\,\text{m}}\times2.3071\times10^{-28}\,\text{J}\,^{\circ}\text{m}\times\left(1-\frac{30}{274}\right)$$

$$= -789 \text{ kJ/mol}$$

7.16   CaO has charges of 2+ and 2–, and radii of 114 and 126 pm, total distance of 240 pm.

KF has charges of 1+ and 1–, and radii of 138 and 119 pm, total distance of 257 pm.

The distance in CaO is 7% smaller and the charge factor is four times as large, both leading to stronger interionic attraction and contributing to the hardness of the crystal.

MgO has charges of 2+ and 2–, and radii of 86 and 126 pm, total distance of 212 pm, with NaCl structure and Madelung constant = 1.75.

CaF_2 has charges of 2+ and 1–, and radii of 126 and 119 pm, total distance of 245 pm with the fluorite structure and Madelung constant = 2.52.

The size difference and charges favor stronger MgO interionic attraction, enough to overcome the Madelung constant difference.

7.17 $MgCl_2$ has a rutile structure, so it will be used for the $NaCl_2$ calculation.

The lattice energy for a rutile structure with combined radii of 253 pm (either $NaCl_2$ or $MgCl_2$) is:

$$U = \frac{NMZ_+Z_-}{r_0}\left[\frac{e^2}{4\pi\varepsilon_0}\right]\left(1-\frac{\rho}{r_0}\right)$$

$$U = \frac{6.022\times10^{23}\,\text{mol}^{-1}\times2.385\times2\times(-1)}{253\times10^{-12}\,\text{m}}\times2.307\times10^{-28}\,\text{Jm}\times\left(1-\frac{30}{253}\right)$$

$$= -2{,}310 \text{ kJ mol}^{-1}$$

The lattice energy of $MgCl_2$ (and the hypothetical $NaCl_2$) is negative. If the Born—Haber cycles of $MgCl_2$ and $NaCl_2$, respectively, were compared, important contributing terms that would differ

would be the ΔH_{sub} and ionization energy values. The magnitudes of the second ionization energies vary tremendously. $Na^+ \rightarrow Na^{2+} + e^-$, removing an electron from a core $2p$ orbital, requires much more energy than the corresponding $Mg^+ \rightarrow Mg^{2+} + e^-$ reaction that removes the second $3s$ valence electron.

The two metals differ by about 2,800 kJ/mol in these steps (all in kJ/mol):

Na $(s) \rightarrow$ Na(g)	107	Mg $(s) \rightarrow$ Mg (g)	147
Na $(g) \rightarrow$ Na$^+(g) + e^-$	495	Mg $(g) \rightarrow$ Mg$^+(g) + e^-$	738
Na$^+ (g) \rightarrow$ Na$^{2+}(g) + e^-$	4562	Mg$^+ (g) \rightarrow$ Mg$^{2+}(g) + e^-$	1451
Totals: Na $(s) \rightarrow$ Na$^{2+}(g) + 2e^-$	5164	Mg $(s) \rightarrow$ Mg$^{2+}(g) + 2e^-$	2336

Therefore, it is extremely unlikely that NaCl$_2$ can be made. The large second ionization energy of Na does not permit the ΔH_f for hypothetical NaCl$_2$ to be negative despite the predicted large and negative lattice energy of this salt.

Repeating the process for a sodium chloride lattice (sum of radii = 274 pm) to compare The lattice energy and the energies necessary to form Na$^+$ and Mg$^+$:

$$U = \frac{NMZ_+Z_-}{r_0}\left[\frac{e^2}{4\pi\varepsilon_0}\left(1 - \frac{\rho}{r_0}\right)\right]$$

$$U = \frac{6.022 \times 10^{23}\,\text{mol}^{-1} \times 1.748 \times 1 \times (-1)}{274 \times 10^{-12}\,\text{m}} \times 2.307 \times 10^{-28}\,\text{Jm} \times \left(1 - \frac{30}{274}\right)$$

$$= -789 \text{ kJ mol}^{-1}$$

Na $(s) \rightarrow$ Na(g)	107	Mg $(s) \rightarrow$ Mg (g)	147
Na $(g) \rightarrow$ Na$^+(g) + e^-$	495	Mg $(g) \rightarrow$ Mg$^+(g) + e^-$	738
Na $(s) \rightarrow$ Na$^+(g) + e^-$	602	Mg $(s) \rightarrow$ Mg$^+(g) + e^-$	885

Unlike with NaCl$_2$, the lattice energy associated with forming MgCl nearly compensates for the energy required to generate Mg^+. From this perspective, the formation of MgCl is more realistic. However, the ionic bonding in MgCl$_2$ is so much stronger (nearly triple the lattice energy) that MgCl is a very unlikely product of the reaction of Mg and Cl_2. Indeed, MgCl$_2$ is the thermodynamic sink in this system.

7.18

½ Br$_2$ $(l) \rightarrow$ ½ Br$_2$ (g)	14.9	(Energies in kJ/mol)
½ Br$_2$ $(g) \rightarrow$ Br (g)	95.1	
Br $(g) + e^- \rightarrow$ Br$^-$	−324.7	
K $(s) \rightarrow$ K (g)	79.0	
K $(g) \rightarrow$ K$^+ + e^-$	418.8	
K$^+ (g) +$ Br$^- (g) \rightarrow$ KBr (s)	−687.7	
Total	−404.6 kJ mol^{-1} for K $(s) +$ ½ Br$_2$ $(l) \rightarrow$ KBr (s)	

For a sodium chloride lattice with total radii of 320 pm:

$$U = \frac{NMZ_+Z_-}{r_0}\left[\frac{e^2}{4\pi\varepsilon_0}\right]\left(1 - \frac{\rho}{r_0}\right)$$

$$U = \frac{6.022\times10^{23}\,\text{mol}^{-1}\times1.748\times1\times(-1)}{320\times10^{-12}\,\text{m}}\times2.307\times10^{-28}\,\text{Jm}\times\left(1 - \frac{30}{320}\right)$$

$$= -687.7\ \text{kJ mol}^{-1}$$

7.19

½ O$_2$ (g) → O (g)	247	(Energies in kJ/mol)
O (g) + 2 e$^-$ → O^{2-}	603	
Mg (s) → Mg (g)	37	
Mg (g) → Mg^{2+}+ 2e$^-$	2188	
Mg^{2+}+ O^{2-}→ MgO (s)	−3934	
Total	−859 kJ mol^{-1} for Mg (s) + ½ O$_2$ (g) → MgO (s)	

For a sodium chloride lattice with total radii of 212 pm:

$$U = \frac{NMZ_+Z_-}{r_0}\left[\frac{e^2}{4\pi\varepsilon_0}\right]\left(1 - \frac{\rho}{r_0}\right)$$

$$U = \frac{6.022\times10^{23}\,\text{mol}^{-1}\times1.748\times2\times(-2)}{212\times10^{-12}\,\text{m}}\times2.307\times10^{-28}\,\text{Jm}\times\left(1 - \frac{30}{212}\right) = -3934\ \text{kJ mol}^{-1}$$

7.20   PbS has total radii of 303 pm. For the NaCl lattice:

$$U = \frac{NMZ_+Z_-}{r_0}\left[\frac{e^2}{4\pi\varepsilon_0}\right]\left(1 - \frac{\rho}{r_0}\right)$$

$$U = \frac{6.022\times10^{23}\,\text{mol}^{-1}\times1.748\times2\times(-2)}{303\times10^{-12}\,\text{m}}\times2.307\times10^{-28}\,\text{Jm}\times\left(1 - \frac{30}{303}\right)$$

$$= -2888\ \text{kJ mol}^{-1}$$

1/8 S$_8$ (s) → S^{2-}(g)	535	(Energies in kJ/mol)
Pb (s) → Pb (g)	196	
Pb (g) → Pb$^+$ (g) + e$^-$	716	
Pb$^+$ (g) → Pb^{2+} (g) + e$^-$	1450	
Pb^{2+} (g) + S^{2-} (g) → PbS (s)	U	

Total   −98 kJ mol^{-1} for Pb (s) + 1/8 S$_8$ (s) → PbS (s)

U = −2995 kJ mol^{-1}, roughly 3.5% more exothermic than -2888 kJ mol^{-1}.

7.21   In ZnO or TiO, additional Zn or Ti would have two more electrons than the metallic ions. As a result, any nonstoichiometry in the direction of excess Zn or Ti would supply extra electrons, making an *n*-type semiconductor.

   In Cu_2S, CuI, or ZnO, excess S, I, or O would have fewer electrons than the corresponding ions. Therefore, the result of excess nonmetals in the lattice would be a *p*-type semiconductor.

7.22   Vibrational motions of the atoms in the lattice become at least partly synchronized, with positive centers moving closer together. This concentration of positive charge can attract electrons, allowing two electrons to be closer to each other than would usually be the case. When the vibrations are synchronized, this attraction can ripple through the material, helping the electrons move. Apparently the whole system acts as if it is at ground state energies, so no net change in energy is needed to keep the process going indefinitely.

7.23   The general reaction is $Na_2Z + Ca^{2+}$ $(aq) \rightarrow CaZ + 2Na^+$ (aq), where Na_2Z is the original zeolite with sodium ions providing the positive charge. When hard water, containing Ca^{2+} or Mg^{2+}, passes through the zeolite, the ions exchange, leaving only Na^+ in the softened water. The zeolite can be regenerated by flushing with concentrated brine. The large Na^+ concentration reverses the reaction above.

7.24   The ion C_2^{4-} should have the following molecular orbitals (see Figure 5.7):
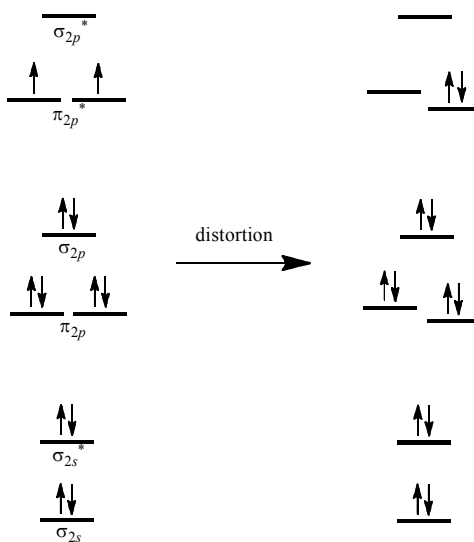
   Distortion could result in removal of the degeneracy of the π_u and π_g^* orbitals, giving a diamagnetic ion.

7.25   Gallium nitride has a larger band gap than gallium arsenide (continuing the trend in which gallium phosphide has a larger band gap than gallium arsenide; see Table 7.3) and emits higher energy light. Gallium nitride has grown rapidly in importance; it is used in high-energy lasers, LEDs that emit light in the high-energy part of the visible spectrum as well as at lower energies, and a variety of other electronics applications.

7.26 The smaller the size of the quantum dots, the greater the separation between energy levels within the dots, and the higher the energy the photoluminescence. Consequently, the largest dots would produce the lowest energy emission bands.

7.27 First appearing in the literature in 2001, articles on medical applications of quantum dots and related topics have been more than doubling in number every two years.

7.28 The spectral effect of the *L*-cysteine/ Cd^{2+} ratio on the absorbance of CdS quantum dots is shown in Figure 1 of this reference. The molar ratio 4:2 causes the highest blue shift of the absorption edge (363 nm) and affords the smallest CdS quantum dots. These QDs absorb UV-Vis radiation of highest energy among those studied in this paper.

7.29 These quantum dots were prepared via first generating a solution of $CdCl_2 \cdot 2.5\,H_2O$ and thiourea in a small volume of ultrapure water. An aqueous solution of 3-mercaptopropionic acid was added, followed by 1 M NaOH, until the pH = 10. The molar ratio of Cd^{2+}/thiourea/3-mercaptopropionic acid was typically 1/1.7/2.3. The solution was saturated with N_2 and transferred to an autoclave. The mixture was subjected to 100 ° C for specified times before being lowered to ambient temperature. The pressure above the sealed solution increased during the reaction. A reaction scheme is provided here:

(Chemicals in autoclave)   (Species in autoclave after the reaction)
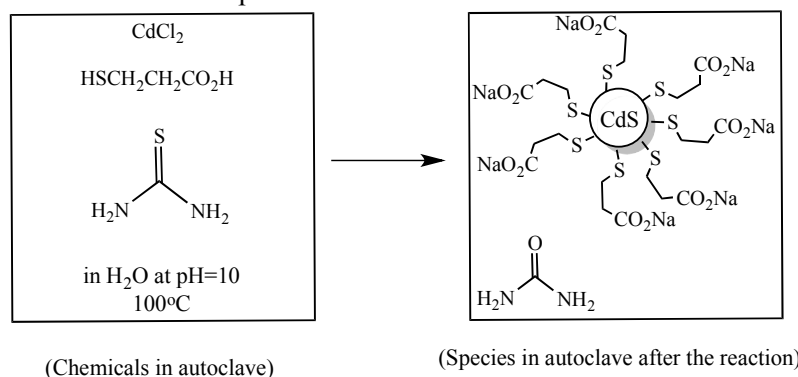
The diameters of these QDs depend on the reaction time, with longer times leading to larger QDs. Diameters were calculated via two mathematical approaches using band gap and UV-Vis data, respectively.

Reaction Time (min)	Diameters (nm) from Band Gap Data	Diameters (nm) from UV-Vis Data
45	2.5(4)	2.3(4)
60	2.7(4)	2.5(4)
90	3.1(4)	2.9(4)
120	3.5(4)	3.1(4)
180	3.9(4)	3.7(4)

As impressively shown in Figures 2b and 2c of the reference, the smaller the QDs (the shorter the reaction time), the higher the energy of the emitted radiation when these QDs are excited with UV radiation. The emission peak maxima vary from 510 nm (smallest QDs, 45 min reaction time) to 650 mn (largest QDs, 180 min reaction time).

7.30   These authors employed two spectroscopic methods to assess CdSe and CdTe quantum dot size. UV-Vis spectra were obtained throughout the digestive ripening stage to monitor particle size. Fluorescence spectra were subsequently acquired to confirm the UV-Vis results. The UV-Vis spectra acquired after 4 and 8 hours of digestive ripening are in Figure 3 of the reference. The corresponding fluorescence spectra are in Figure 4. The lower energy fluorescence λ_{max} of the CdTe QDs (572 nm) relative to that of the CdSe QDs (530 nm) indicates the larger size of the CdTe QDs (Figure 4). A fundamental concept for QDs, that decreasing size leads to higher-energy emitted radiation, is applied to make the size assessment. The relative sizes were further examined by transmission electron microscopy (TEM) experiments that indicated the average particle sizes of the CdSe and CdTe QDs to be 4.0 and 4.5 nm, respectively.

7.31   The metallic nature of $BaGe_3$ was probed by measuring the temperature dependence of its electrical resistivity; the metallic nature was established since the resistivity decreases with decreasing temperature. Zero resistivity was observed below 4.0 K, suggesting that $BaGe_3$ is a superconductor with this critical temperature. The Meissner effect was also observed at 4.0 K, providing further support of this critical temperature.

The conduction bands of $BaGe_3$ are mainly composed of Ge $4p$ orbitals with some contribution from Ba orbitals. The states near the Fermi level are primarily made up of Ge $4p$ and Ba $5d$ orbitals. It is interesting that the Ge $4p_x$, $4p_y$, and $4p_z$ orbitals contribute to different relative extents to the conduction bands near the Fermi level, with large contributions of Ge $4p_x$ and $4p_y$ orbitals near the Fermi level of $BaGe_3$.

7.32   Figure 3 of the reference provides a plot of T_c versus a-axis lattice constants. For the LnFeAsO-based materials, the highest T_c is associated with an a-axis lattice constant of approximately 3.91 Å. The T_c values reach a maximum when the lanthanide element lies roughly in the middle of the lanthanide series (Sm, Gd), and decreases as the masses of the lanthanide atoms increase and decrease, respectively, from these elements, with La, Ce, (the lightest lanthanides) and Er (a heavier lanthanide) lying at the extremes of the T_c curve for LnFeAsO-based materials. In this regard, a periodic trend is roughly observed.

The authors suggest an upper limit on the a-axis constant (~4.0 Å) for the possibility of superconductivity. The lack of superconductivity of the two perovskite-based As materials ($(Sr_3Sc_2O_5)(Fe_2As_2)$ and $(Ba_3Sc_2O_5)(Fe_2As_2)$) is attributed to their very long a-axis constants of roughly 4.07 and 4.13 Å, respectively.

7.33   **a.** $Si_4O_{12}^{8-}$

b. $Si_8O_{24}^{16-}$

c. $[Si_6O_{17}^{10-}]_n$